

# MARA-Net: Single Image Deraining with Multi-level Connections and Adaptive Regional Attentions

Yeachan Park, Myeongho Jeon, Junho Lee and Myungjoo Kang  
 Seoul National University, Seoul, Republic of Korea  
 1 Gwanak-ro, Gwanak-gu, Seoul, Republic of Korea  
 {ychpark, andyjeon, joon2003, mkang}@snu.ac.kr

## Abstract

*Removing rain streaks from single images is an important problem in various computer vision tasks because rain streaks can degrade outdoor images and reduce their visibility. While recent convolutional neural network-based deraining models have succeeded in capturing rain streaks effectively, difficulties in recovering the details in rain-free images still remain. In this paper, we present a multi-level connection and adaptive regional attention network (MARA-Net) to properly restore the original background textures in rainy images. The first main idea is a multi-level connection design that repeatedly connects multi-level features of the encoder network to the decoder network. Multi-level connections encourage the decoding process to use the feature information of all levels. Channel attention is considered in multi-level connections to learn which level of features is important in the decoding process of the current level. The second main idea is a wide regional non-local block (WRNL). As rain streaks primarily exhibit a vertical distribution, we divide the grid of the image into horizontally-wide patches and apply a non-local operation to each region to explore the rich rain-free background information. Experimental results on both synthetic and real-world rainy datasets demonstrate that the proposed model significantly outperforms existing state-of-the-art models. Furthermore, the results of the joint deraining and segmentation experiment prove that our model contributes effectively to other vision tasks.*

## 1. Introduction

Adverse weather conditions such as rain, haze, and snow, can produce complex visual effects on natural images and videos. In particular, rain streaks, which is one of the most commonly occurring phenomena in outdoor imaging, can potentially degrade the performance in several computer vision applications. Therefore, it is imperative to develop

algorithms that effectively remove rain streaks and restore pristine background scenes in vision-related tasks.

Over the past few decades, several research works have studied the removal of rain streaks from captured images. Several traditional deraining methods [1, 2, 4, 14, 18, 21] have been suggested to separate rain streaks from the clean background image based on the physical characteristics or texture appearance patterns of the rain streaks. Recently, convolutional neural network (CNN)-based methods have achieved great success in solving this problem [8, 9, 15, 16, 17, 23, 24, 26, 30, 33, 37, 38, 42, 45].

Although most existing deraining methods exhibit remarkable performance in capturing rain streaks, they have difficulties in recovering the missing details in the background.

Wang *et al.* [30] and Yu *et al.* [42] utilize an encoder-decoder U-Net-like architecture as a rain-to-clean image translation model. However, connections between inter-level features are not considered, although skip connections within the same level are applied. This kind of model design can lead to information loss due to the lack of communication between different levels. To address this issue, Jiang *et al.* [13] exploits multi-scale fusions to represent rain streaks across multiple scales. However, these fusions lack interactivity because only the connections from smaller to larger scales are considered.

Li *et al.* [15] and Yu *et al.* [42] successfully fuse local and global information by exploiting regional non-local operations. These models use a square grid with the same aspect ratio in non-local operations. However, the operations with the square grid lack an understanding of the unique properties of the rain streaks because of their vertical distribution in the rainy image, which we explore (see Figure 3). Consequently, these methods have difficulties in recovering details in extremely adverse weather conditions.

To address the above-mentioned issues, we present a multi-level connection and adaptive regional attention network (MARA-Net) to carefully remove rain streaks and recover background details using multiple scale features in

rainy images. The proposed MARA-Net is based on a U-Net-like [25] architecture consisting of down-sampling and up-sampling components as depicted in Figure 1.

Inspired by [27, 28, 32], we construct multi-level connections between multiple-scale features to efficiently utilize information across various scales in the recovery of the background. Unlike [13], we implement an interactive multi-connection that considers the interconnections between different scales. Because the features at multiple levels show different scale characteristics, direct connections can cause adverse effects in the model. To adaptively rescale the channel-wise features in the multi-level connections, we apply a channel-wise attention layer [11] after the multi-level connection, which helps the network to focus on the useful channels.

In addition, we implement a non-local operation [34] to capture long-range spatial dependencies between distant pixels. We propose a wide regional non-local block (WRNL), which divides feature maps into grids of wide regions (see Figure 2) before performing the region-wise non-local operation. This wide grid provides a relatively more even distribution of the rain streaks by region, which facilitates the retrieval of rich long-range background information during the recovery of the original rain-free image (see section. 3.2.1).

Additionally, as described in [37], to prevent information loss during the sampling operation, we adopt the discrete wavelet transform (DWT) and inverse DWT (IWT) in place of the simple pooling and de-convolution operations. Unlike the pooling operation, the DWT operation is invertible via IWT, which helps to avoid information loss. In addition, rain streaks can be captured with rich frequency information via wavelet transform. Finally, we adopt a new data augmentation strategy called CutMix [43], which replaces small patches of the rainy image with corresponding parts of the ground-truth rain-free image. This provides a generalization effect with characteristics similar to those of regional dropout.

We evaluate the proposed MARA-Net on five synthetic and two real-world deraining datasets and compare its performance with existing state-of-the-art methods. In summary, the contributions of this work may be summarized as follows.

- 1) We propose novel multi-level connections between levels to restore the details of the image. At each stage of the up-sampling part of the network, feature information of all the scales in the down-sampling part is aggregated. By rescaling the features of multiple levels channel-wise, we effectively aggregate different scale characteristics.

- 2) We propose the WRNL, which effectively restores the background by using sufficient rain-free information in each region of widely divided grids in the input feature maps.

- 3) We perform experiments on both synthetic and real-

world rain datasets and demonstrate that the proposed method significantly outperforms existing state-of-the-art methods. In particular, MARA-Net exhibits remarkable performance on SPA-Data, the real-world rain dataset considered in this study.

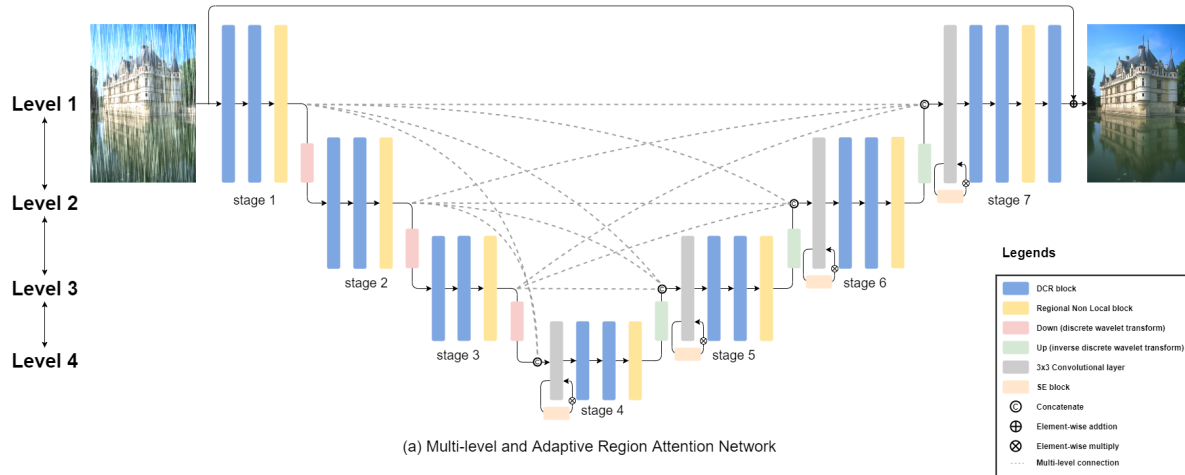
- 4) We construct joint image deraining and semantic segmentation models on the RainCityscape dataset. In addition to conventional comparisons such as the peak signal-to-noise ratio (PSNR) and structural similarity index measure (SSIM), we comprehensively evaluate the contribution of the deraining model to other vision tasks.

## 2. Related Work

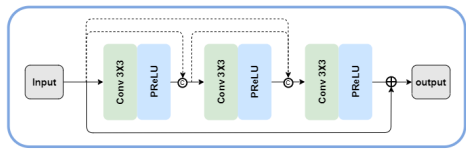
The single image deraining problem begins with the assumption that a rainy image consists of a background layer and a rainy layer. Several traditional training methods based on single images and videos have been proposed. Barnum *et al.* [1] reconstruct rainy images by combining the appearance model with the streak model. The appearance model identifies individual rain streaks and the streak model utilizes the statistical characteristics of rain. Chen and Hsu [4] use the low-rank model to separate the layers in a rainy image. As noted by Yang *et al.* [39], sparse coding is applied during this process to separate the rainy layer from the rainy image [6, 14, 21, 35, 48]. Further, Li *et al.* [2, 18] approach this problem using the Gaussian mixture model.

Because of the remarkable performance exhibited by deep learning-based methods, especially CNN-based ones, the potential use of deep learning in deraining has been extensively researched. Yang *et al.* [38] apply a CNN-based method for the first time and express natural images by adding atmospheric light as a component to rainy images. Fu *et al.* [9] and Fan *et al.* [8] use a single primary network that restores input images using the residual network. Based on the residual network, Li *et al.* [17] attempt to further eliminate overlapping rain streaks by organizing the context aggregate network into multiple stages. Shen *et al.* [26] consider rain streaks to be high-frequency and attempt to remove rain streaks by utilizing DWT. Yang *et al.* [37] divide the deraining process into several stages and reconstruct the image recurrently, beginning with a small portion of the image to eventually obtain the entire image.

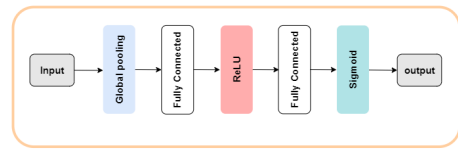
Wang *et al.* [33] capture the spatial contextual information using a four-directional recurrent neural network with the identity matrix initialization model. Ren *et al.* [24] propose progressive ResNet to effectively remove the rain via recursive computation. Yu *et al.* [42] propose GraNet, which is designed to identify rain masks in the coarse stage using a region-aware non-local block. Subsequently, the process uses the rain masks to create the final image using another reconstruction network. To achieve pixel-wise deraining in image recovery, encoder-decoder structures have been used in certain methods. Wang *et al.* [30] propose the



(a) Multi-level and Adaptive Region Attention Network



(b) DCR Block



(c) SE Block

Figure 1. Overview of the proposed MARA-Net structure.

residual learning branch as a component of the encoder. Li *et al.* [15] enhance the performance by introducing non-local blocks into the encoder-decoder network. Among the methods that reconstruct the rainy layer to be identical to the background layer, the generative adversarial network is widely used to remove raindrops and rain streaks [16, 23, 45].

Yang *et al.* [40] propose the fractal band learning network based on frequent band recovery. Wang *et al.* [31] propose an interpretable deep network based on a convolutional dictionary network. Jiang *et al.* [13] use the images of various sizes as the input to the model. A multi-scale pyramid structure is used to promote cooperative representation. Deng *et al.* [7] propose two-branch parallel networks, in which one branch performs rain removal and the other branch detail recovery. In [36], newly formulated rain streaks transmission maps, vapor transmission maps, and atmospheric lights are respectively learned by three different networks. Zhang *et al.* [46] propose a paired rain removal network, which exploits both stereo images and semantic information.

### 3. Proposed Network

In this section, we describe the architecture of the proposed MARA-Net, which is capable of properly removing rain streaks and retaining the background details of the image in both synthetic and real-world datasets. MARA-Net is based on a U-Net-like structure whose overview is depicted in Figure 1. As is apparent from the figure, we divide the

levels according to the size of the feature map and define a set of blocks as a stage.

The proposed MARA-Net consists of an encoder part and a decoder part. The first three stages form the encoder part, and the remaining four stages the decoder part. We propose multi-level connections, which connect all outputs of the encoder to all inputs of the decoder. These multi-level connections enable more diverse scale features to be used during the restoration process. Each stage of MARA-Net is composed of two densely connected residual (DCR) blocks, each of which consists of three convolution layers followed by PReLU [29] (refer Figure 1(b)) and one WRNL block. To adaptively rescale channel-wise features after concatenating the multi-level connections, a squeeze-and-excitation (SE) block is added in front of each decoder stage. A  $1 \times 1$  convolutional layer follows the SE block to adjust the number of channels.

#### 3.1. Multi-Level Connections

**Squeeze-and-Excitation Block** The idea of channel-wise attention has been widely used in CNNs to utilize channel-wise dependencies between features. The SE network [11] is adopted in the proposed network to rescale channel-wise features. In SENet, channel-wise statistics are obtained via global average pooling (GAP) to exploit global contextual information lying outside the local receptive regions. To fully capture channel-wise dependencies, a gating mechanism is introduced to form two fully-connected (FC) layers that reduce or increase the dimensionality with the ratio  $r$ . Following [47], we incorporate the idea of the

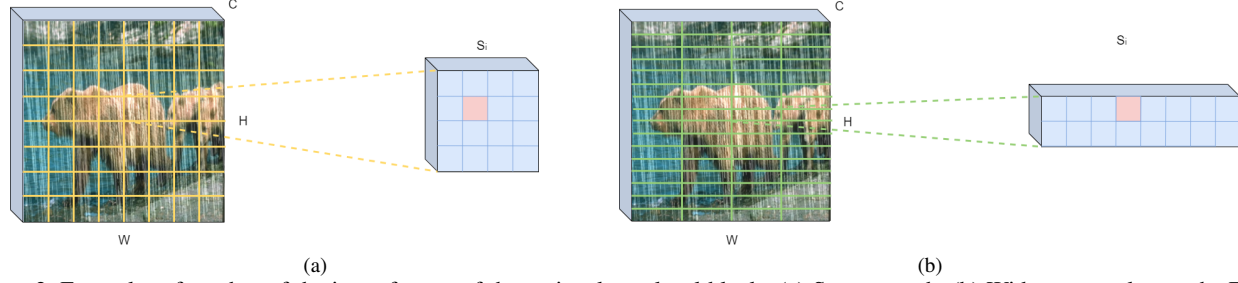


Figure 2. Examples of patches of the input feature of the regional non-local block. (a) Square patch, (b) Wide rectangular patch. Every pixel in a patch refers to every pixel in the patch.

residual block [19] with channel-wise attention (see Figure 1) to construct the SE block.

Formally, given an input feature map  $X$ , the SE Block  $f_{SE}(\cdot)$  can be expressed as follows:

$$S = \sigma(W_2 \delta(W_1 H_{GAP}(X))) \quad (1)$$

$$f_{SE}(X) = X + \hat{X} = X + S \otimes_c X \quad (2)$$

where  $\otimes_c$  denotes channel-wise multiplication,  $H_{GAP}(\cdot)$  denotes the global average pooling function,  $\sigma$  denotes the sigmoid function,  $\delta$  denotes the ReLU function,  $W_1 \in \mathbb{R}^{\frac{C}{r} \times C}$  and  $W_2 \in \mathbb{R}^{C \times \frac{C}{r}}$  denote the dimension reduction and dimension-increasing FC layers respectively, and  $r$  denotes the reduction ratio in the gating mechanism.

**Multi-Level Connections** In the usual U-Net-like network, connections exist only between features corresponding to the same level. Such a structure cannot make use of multiple scale information during the recovery of low-level features in the decoder. However, single image de-raining is a low-level vision task that requires richer range scale features to restore the details in the image. Inspired by [27, 28, 32], we formulate multi-level connections to aggregate the features of all the levels. At each stage of the up-sampling part of the network, feature information from all scales in the down-sampling part is aggregated. Because the features of multiple levels have different scale characteristics, we adopt the SE block to adaptively rescale the channel-wise features.

Formally, let  $E_{out}^l$  be the output features at level  $l$  ( $l = 1, 2, 3$ ) in the encoder part. At each level  $l$  ( $l = 1, 2, 3, 4$ ) in the decoder part, the input feature  $D_{in}^l$  is given as:

$$D_{concat}^l = \left( \bigoplus_{i=1}^3 H_i^l(E_{out}^i) \right) \oplus H_{up}(D_{out}^{l+1}) \quad (3)$$

$$D_{in}^l = W_{1 \times 1}(f_{SE}(D_{concat}^l)) \quad (4)$$

where  $\oplus$  denotes the concatenation operation,  $H_{up}(\cdot)$  denotes the up-sampling operation,  $D_{out}^l$  denotes the output feature of the decoder part at level  $l$ ,  $W_{1 \times 1}$  denotes the  $1 \times 1$  convolution layer, and  $f_{SE}(\cdot)$  denotes the SE block discussed above.  $H_i^l(\cdot)$  denotes the sampling operation from

level  $i$  to  $l$ . In other words,  $H_i^l$  is the down-sampling by  $l - i$  times, identity, and up-sampling by  $i - l$  times operations if  $l > i$ ,  $l = i$ , and  $l < i$ , respectively. We set  $D_{in}^5 = 0$  for convenience.

Without multi-level connections, high-level features cannot be used during the processing of low-level features and vice versa. This approach helps the network to exploit various scale representations in recovering large-scale features. To find the correct correspondence between the feature shapes at different scales, we apply discrete wavelet transforms (DWT or IWT), as described in Section 3.3, for the down-sampling and up-sampling operations.

### 3.2. Wide Regional Non-Local Block

In this section, we first describe the representation of the WRNL block and then provide an analysis of the effectiveness of the WRNL block based on statistical exploration.

We denote the input feature to the WRNL as  $X \in \mathbb{R}^{H \times W \times C}$ . We divide  $X$  into a  $a \times b$  grid of patches  $\{X^k\}$ , ( $k = 1, \dots, K = ab$ ) where  $K$  is the number of patches. The grid division is illustrated in Figure 2. The linear embedding processes for  $X^k$  to generate the output  $Z^k$  are formulated as follows.

$$\Phi(X^k)_i^j = \phi(X_i^k, X_j^k) = \exp\{\theta(X_i^k)\psi(X_j^k)^T\} \quad (5)$$

$$\theta(X_i^k) = X_i^k W_\theta, \psi(X_i^k) = X_i^k W_\psi, G(X)_i^k = X_i^k W_g \quad (6)$$

where  $X_i^k$  and  $X_j^k$  denote the feature  $X^k$  at position  $i$  and  $j$ , respectively. The learnable weight matrices  $W_\theta$ ,  $W_\psi$ , and  $W_g$  have the dimensions of  $C \times L$ ,  $C \times L$ , and  $C \times C$ , respectively. In practice,  $L = C/2$  is used. The regional non-local operation can be expressed as follows:

$$Z_i^k = \frac{1}{\delta_i(X^k)} \sum_{j \in S_i} \Phi(X^k)_i^j G(X^k)_i, \quad \forall i, \quad (7)$$

where  $\delta_i(X^k) = \sum_{j \in S_i} \phi(X_i^k, X_j^k)$  denotes the correlation between  $X_i^k$  and each  $X_j^k$  in  $S_i$ , and  $Z_i^k$  denotes the output feature  $Z^k$  at position  $i$ .  $S_i$  denotes a set of patch positions. If  $a > b$ , then the patch is wider than when  $a = b$ . Therefore, we call the patch a wide rectangular patch, a square

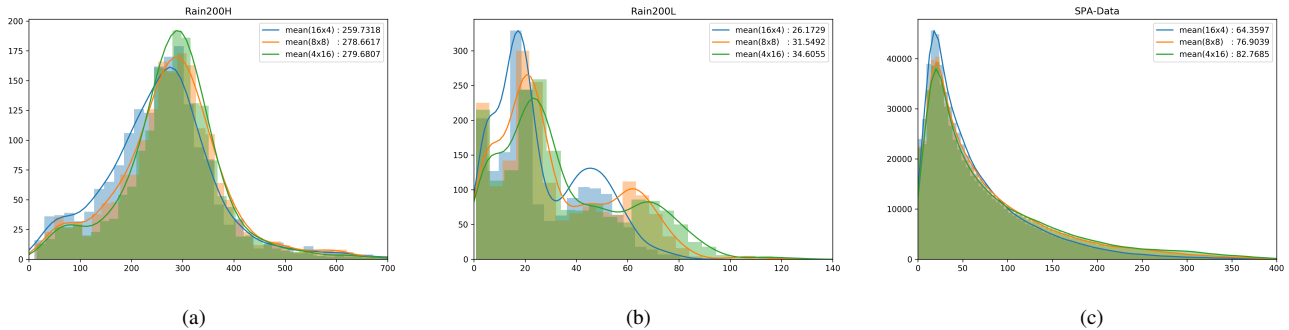


Figure 3. Analysis of rain streak distributions in various region types. (a) Rain200H [38], (b) Rain200L [38], and (c) SPA-Data [33]. The x-axis represents the standard deviation between the number of rain pixels in the patches in each image. The y-axis represents the number of images. The distribution of the images according to the standard deviation is represented by histograms. We approximate the probability density function of the histogram by using kernel density estimation.

patch, and a tall rectangular patch if  $a > b$ ,  $a = b$ , and  $a < b$ , respectively. In the WRNL block, we set the  $a \times b$  grids to  $16 \times 4$ ,  $8 \times 2$ ,  $4 \times 1$ , and  $4 \times 1$  at levels 1, 2, 3, and 4, respectively.

### 3.2.1 Analysis

Given that the non-local block recovers a specific pixel based on the information of other pixels in the patch, it is necessary to have sufficient background information in each patch. The regional non-local block uses the background information sufficiently if the rain streaks are evenly distributed between the patches. However, we observe that the rain streaks are not evenly distributed between square patches in the images used in the previous deraining research [15, 42]. Because of the predominantly vertical distribution of rain streaks, we expect that wide rectangular patches have a more even distribution of the streaks than square and tall rectangular patches.

The distribution of the rain streaks is confirmed through experiments. Wide rectangular, square, and tall rectangular patches are prepared by dividing the height and width of the image into  $16 \times 4$ ,  $8 \times 8$  and  $4 \times 16$  grids respectively. It should be noted that (a) in Figure 2 contains an  $8 \times 8$  grid of patches, and (b) in Figure 2 contains  $16 \times 4$  grid of patches. We consider pixels as rain streaks if the difference between the pixels in  $x_{input}$  and  $x_{gt}$  exceeds a certain threshold. The standard deviation between the number of rain pixels in the patches included in each image is depicted in Figure 3. Wide rectangular patches are observed to exhibit smaller standard deviation values compared to square and tall rectangular patches, which implies an even distribution of rain across all patches. This results in the effective recovery of the image because the usable background information within each patch is also distributed evenly as shown in Table 4.

### 3.3. Discrete Wavelet Transform

The proposed network uses DWT and IWT for down-sampling and up-sampling, respectively. In particular, we adopt the Haar transform, which is simple and widely used method in image processing [10, 20, 22, 26, 37]. The Haar transform is calculated based on the filter  $f_{LL}$ ,  $f_{LH}$ ,  $f_{HL}$  and  $f_{HH}$  as follows:

$$f_{LL} = \frac{1}{4} \begin{bmatrix} 1 & 1 \\ 1 & 1 \end{bmatrix}, f_{LH} = \frac{1}{4} \begin{bmatrix} -1 & -1 \\ 1 & 1 \end{bmatrix}, f_{HL} = \frac{1}{4} \begin{bmatrix} -1 & 1 \\ -1 & 1 \end{bmatrix}, f_{HH} = \frac{1}{4} \begin{bmatrix} 1 & -1 \\ -1 & 1 \end{bmatrix}. \quad (8)$$

Given that  $f_{LL}$  is identical to average pooling,  $LL$  achieves local translation invariance by reducing the size of the feature map (Equation 8).  $LH$ ,  $HL$ , and  $HH$  contain edge information. In particular, as  $LH$  contains vertical edge information, the features of the rain streaks can be effectively obtained from it. The IWT operation during the up-sampling process is the inverse operation of the DWT.

### 3.4. Data Augmentation

In addition to commonly adopted data augmentation techniques such as random cropping and horizontal flipping, we utilize the CutMix [43] augmentation strategy which cuts and pastes ground-truth patches onto input images. In visual recognition, CutMix helps the model to use pixels efficiently and achieve regularization. Yoo *et al.* [41] demonstrate that this approach is also useful in low-level vision tasks, such as image super-resolution. Denoting the input and ground truth as  $x_{input}$  and  $x_{gt}$ , respectively, we perform the CutMix operation as follows:

$$\tilde{x} = \mathbf{M} \odot x_{input} + (\mathbf{1} - \mathbf{M}) \odot x_{gt} \quad (9)$$

where  $\mathbf{M}$  denotes the binary mask, that indicates the location of the replacement,  $\mathbf{1}$  denotes the binary mask filled with ones, and  $\tilde{x}$  and  $\odot$  denote the augmented sample and element-wise multiplication, respectively. We randomly sample the size of the binary mask  $\mathbf{M}$  while keeping it smaller than half of the input image.

### 3.5. Loss Function

We define the loss function  $L$  as follows.

$$\mathcal{L} = \|x_{gt} - f(x_{input})\|_1 + \|x_{gt} - f(x_{input})\|_2 \quad (10)$$

where  $x_{input}$  denotes the input rainy image,  $x_{gt}$  denotes the corresponding rain-free image, and  $f$  denotes the return of the MARA-Net output with respect to  $x_{input}$ .

Table 1. Synthetic and real-world datasets

Datasets	Train	Test	Type
Rain200L [38]	1,800	200	synthetic
Rain200H [38]	1,800	200	synthetic
Rain800 [45]	700	100	synthetic
Rain1200 [44]	12,000	1,200	synthetic
RainCityscapes [5, 12]	9,432	1,188	synthetic
SPA-Data [33]	640k	1,000	real-world
Yang <i>et al.</i> [38]	-	15	real-world

## 4. Experiments

In this section, we present the dataset used in this study and describe the details of the experimental setting. We conduct a quantitative and qualitative evaluation of the proposed method and compare its performance with state-of-the-art methods. An ablation study is conducted to confirm the significance of each component introduced in Section 3.

### 4.1. Experiment Details

For all the datasets, we randomly crop  $256 \times 256$  patch from each input image. During the training, we set the batch size to 4 and use the Adam optimizer. For the Rain200H, Rain200L, and Rain800 datasets, we train our model for 200 epochs. For the Rain1200 and the RainCityscapes datasets, we train our model for 100 epochs. For the SPA-Data dataset, we train our model for 3 epochs.

### 4.2. Datasets and Evaluation Metrics

Five synthetic datasets and two real-world datasets are used to evaluate the performance of the proposed method (see Table 1). As pointed out by Ren *et al.* [24], certain overlaps of background exist between the training and test datasets in the Rain100H and Rain100L datasets. Therefore, we evaluate our model using the updated Rain200H and Rain200L datasets, which do not share backgrounds with the corresponding training datasets.

Because the absence of ground truth data makes quantitative evaluation impossible, the real-world dataset of Yang *et al.* [38] is evaluated qualitatively using the Rain200H-trained weights. We compare the performance of the proposed method with seven state-of-the-art single-image deraining methods.

### 4.3. Results on Synthetic Datasets

As mentioned in Section 4, the proposed MARA-Net is evaluated on four synthetic datasets [33, 38, 45], and the performance is compared to seven state-of-the-art methods [7, 17, 24, 31, 33, 38, 39]. The quantitative results on the synthetic datasets are presented in Table 2. As is evident from the data, the proposed MARA-Net achieves remarkable the improvement over existing state-of-the-art methods with respect to the PSNR and SSIM metrics across all datasets. The original inputs, the ground truth, and the qualitative results for Rain200H are shown in Figure 4. As is evident from Figure 4, JORDER [38], RESCAN [17], and SPANet [33] fail to remove the rain streaks from the heavy rain images. PReNet [24], ReHEN [39] and RCDNet [31] remove almost all the rain streaks from the heavy rain images, but they fail to reconstruct the details of the background. On the other hand, it is apparent that MARA-Net successfully removes all the rain streaks and reconstruct the background more effectively than the other state-of-the-art methods.

### 4.4. Results on Real-world Datasets

For further general verification of the proposed method, additional experiments are conducted on two real-world datasets [33, 38]. On the SPA-Data [33], MARA-Net exhibits quantitatively superior performance compared to the other state-of-the-art methods [7, 17, 24, 31, 33, 38, 39]. The qualitative evaluation is based on the degree to which the rain streaks are removed and the quality of the restored background, as in Section 4.3. Most methods [7, 24, 31, 33, 38] are incapable of completely erasing the actual rain, but the images obtained via RCDNet [31], ReHEN [39] and MARA-Net are almost identical to the ground-truth, as shown in Figure 5.

To confirm the effectiveness of the method trained using synthetic rainy images in removing real rain streaks, qualitative experiments are conducted on real-world rainy images. To compare the model performances under fair conditions, only Rain200H [38] is used during the training process. As shown in Figure 6, MARA-Net generates satisfactory results with respect to both the removal of the rain streaks and the restoration of the details in the background.

### 4.5. Applications for Other Tasks

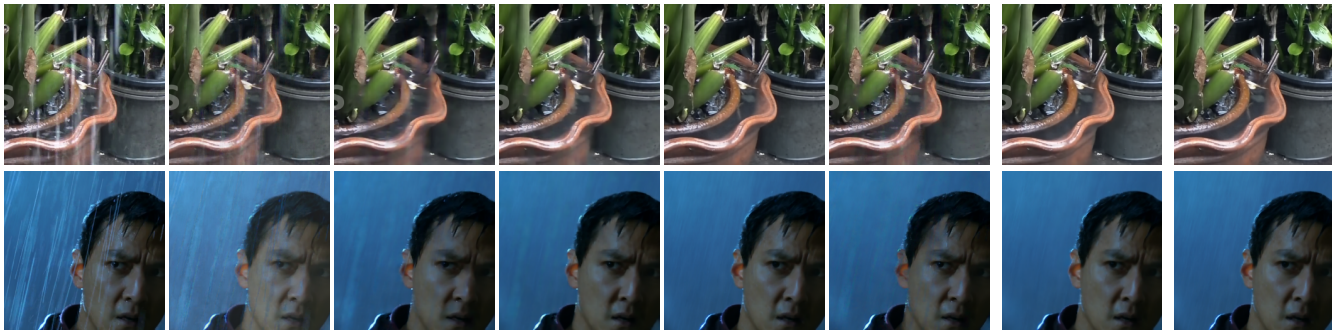
We investigate the effect of the deraining model on improving the performance of high-level vision applications such as semantic segmentation. Because rain streaks can degrade the visibility of objects under complex weather conditions, the incorporation of effective image enhancement would be helpful in several vision models. To this end, we apply the public semantic segmentation model DeepLabV3+ [3] on the Cityscape dataset [5]. Hu *et al.* [12] synthesized rain streaks on the Cityscape dataset with

Table 2. Average PSNR and SSIM comparison on the synthetic datasets Rain200H [38], Rain200L [38], Rain800 [45], Rain1200 [44], and real-world dataset SPA-Data [33]. The highest values are indicated in **red** and the second-highest values are indicated in **blue**. Based on the results, we conclude that the proposed MARA-Net exhibits the best performance on all datasets. In particular, it should be noted that MARA-Net exhibits an overwhelmingly superior performance on the SPA-Data [33] real-world dataset compared to the other state-of-the-art methods.

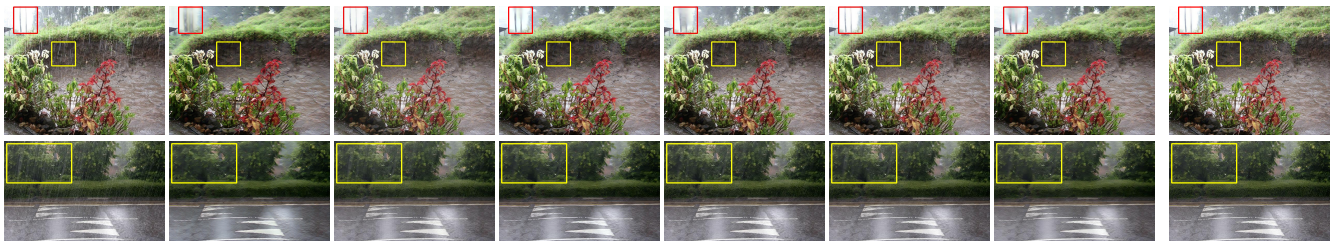
Method	JORDER [38] (CVPR' 2017)	RESCAN [17] (ECCV' 2018)	SPANet [33] (CVPR' 2019)	PRNet [24] (CVPR' 2019)	ReHEN [39] (MM' 2019)	RCDNet [31] (CVPR' 2020)	DRD-Net [7] (CVPR' 2020)	MARA-Net (our)
Rain200L [38]	36.95/0.979	36.94/0.980	35.60/0.974	36.28/0.979	<b>38.57/0.983</b>	35.28/0.971	37.15/0.987	<b>39.73/0.988</b>
Rain200H [38]	22.05/0.727	26.62/0.841	26.32/0.858	27.64/0.884	27.48/0.863	26.18/0.835	<b>28.16/0.920</b>	<b>30.70/0.922</b>
Rain800 [45]	22.24/0.776	24.09/0.841	24.37/0.861	22.83/0.790	<b>26.96/0.854</b>	24.59/0.821	26.32/0.902	<b>28.42/0.876</b>
Rain1200 [44]	24.32/0.862	32.48/0.910	32.38/0.920	30.40/0.891	32.64/0.914	<b>33.54/0.913</b>	-	<b>33.70/0.928</b>
SPA-Data [33]	35.72/0.978	36.99/0.967	38.53/0.987	35.68/0.942	38.65/0.974	<b>41.47/0.983</b>	-	<b>46.88/0.991</b>



(a) Rainy image (b) JORDER [38] (c) RESCAN [17] (d) SPANet [33] (e) PRNet [24] (f) ReHEN [39] (g) RCDNet [31] (h) MARA-Net(our) (i) GT  
Figure 4. Results obtained via several state-of-the-art methods on the Rain200H [38] images. The outputs of MARA-Net exhibit no traces of rain streaks on both image samples. MARA-Net also recovers the most detailed images.



(a) Rainy image (b) RESCAN [17] (c) SPANet [33] (d) PRNet [24] (e) ReHEN [39] (f) RCDNet [31] (g) MARA-Net (our) (h) GT  
Figure 5. Results obtained via several different methods on SPA-Data [33] images. The results from the proposed MARA-Net exhibit almost no traces of rain streaks on both image samples, while the results obtained via the other methods [17, 24, 31, 33, 39] exhibit traces of rain streaks.



(a) Rainy image (b) JORDER [38] (c) RESCAN [17] (d) SPANet [33] (e) PRNet [24] (f) ReHEN [39] (g) RCDNet [31] (h) MARA-Net (our)  
Figure 6. Results obtained via several different methods on real images. For fairness, all methods are trained using only the Rain200H training image pairs.

different rain intensities  $\alpha$  ( $\alpha \in \{0.01, 0.02, 0.03\}$ ). Quantitative results for the improvement of the semantic segmentation accuracy in addition to the deraining performance are reported in Table 5. The qualitative comparison is shown in Figure 7.

#### 4.6. Ablation Study

We conduct an ablation study to demonstrate the significance of all the methods used in the proposed MARA-Net architecture. The Rain200H dataset is used for the ablation study. We conduct three experiments corresponding to each

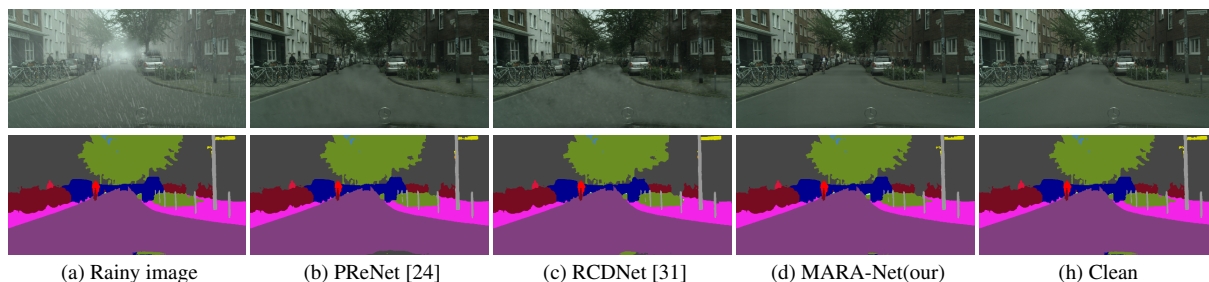


Figure 7. Examples of joint deraining and semantic segmentation. The first row denotes the deraining results on the RainCityscape dataset. The second row denotes the semantic segmentation results obtained by DeepLabV3+ [3].

Table 3. Ablation study on the various strategies presented in Section 3. MLC denotes multi-level connection.

WRNL	DWT	MLC	Cutmix	PSNR	SSIM
				29.12	0.906
✓				29.49	0.911
✓	✓			30.22	0.917
✓	✓	✓		30.62	0.921
✓	✓	✓	✓	30.70	0.922

Table 4. Ablation study on region types of Regional Non-Local Blocks.

Region Type	PSNR	SSIM
Tall Rectangle	29.95	0.915
Square	30.12	0.916
Wide Rectangle	30.22	0.917

Table 5. Comparison results of joint deraining and semantic segmentation on RainCityscape dataset comprising three rain intensities ( $\alpha \in \{0.01, 0.02, 0.03\}$  where  $\alpha$  denotes the intensity of the rain streaks). We use DeepLabV3+ [3] for semantic segmentation. We compare the models that show an improvement in the semantic segmentation performance which is measured as mIOU metric. avg. in the metric column denotes average value of all  $\alpha$ .

Metric	Rainy	PReNet	RCDNet	MARA-Net	Clean
PSNR	15.55	28.88	25.51	<b>35.82</b>	$\infty$
SSIM	0.826	0.972	0.958	<b>0.987</b>	1.000
mIOU					
(avg.)	0.6254	0.7636	0.7402	<b>0.7728</b>	0.7810
( $\alpha=0.01$ )	0.6724	0.7765	0.7641	<b>0.7773</b>	
( $\alpha=0.02$ )	0.6284	0.7652	0.7439	<b>0.7750</b>	
( $\alpha=0.03$ )	0.5777	0.7492	0.7140	<b>0.7663</b>	

of the three settings and report the average of the evaluation values.

**Ablation study on strategies employed.** An ablation investigation is conducted to evaluate the performance of the proposed strategies. The baseline model with a U-Net-like structure for comparison is constructed with two DCR blocks corresponding to each stage and the  $2 \times 2$  max pooling operation and pixel shuffle operation are adopted as the down-sampling and up-sampling operations, respectively. As evident from Table 3, each strategy contributes to the

performance improvement.

**Ablation study on non-local block region types.** To compare the performance of our proposed WRNL block, we evaluate the performance using square, tall, and wide-type regional non-local blocks. The results presented in Table 4 demonstrate that the wide-type regional non-local block achieves the best performance. This demonstrates that the wide-type region is advantageous for the restoration of the rain-free background, because of the even distribution of rain streaks between the regions, as explained in Figure 3.

## 5. Conclusion

In this study, we propose the multi-level connections and an adaptive regional attention network (MARA-Net) for single-image deraining. MARA-Net aggregates features via connections between multiple levels in the background recovery. The SE block following the multi-level connections considers channel-wise attention to effectively aggregate different scale characteristics. To utilize rich long-range rain-free background information in the deraining process, we propose a novel WRNL. An in-depth analysis of rainy images provides the basis for the effective functioning of the WRNL.

The proposed method significantly outperforms existing state-of-the-art methods. In particular, the proposed network satisfactorily restores the details of the input image and almost completely removes rain streaks on both the synthesized and the real-world datasets. Furthermore, additional experiments demonstrate that MARA-Net contributes to other vision tasks by effectively enhancing images degraded under bad weather conditions.

## References

- [1] Peter C Barnum, Srinivasa Narasimhan, and Takeo Kanade. Analysis of rain and snow in frequency space. *International journal of computer vision*, 86(2-3):256, 2010.
- [2] Jérémie Bossu, Nicolas Hautière, and Jean-Philippe Tarel. Rain or snow detection in image sequences through use of a histogram of orientation of streaks. *International journal of computer vision*, 93(3):348–367, 2011.



- [3] Liang-Chieh Chen, Yukun Zhu, George Papandreou, Florian Schroff, and Hartwig Adam. Encoder-decoder with atrous separable convolution for semantic image segmentation. In *Proceedings of the European conference on computer vision (ECCV)*, pages 801–818, 2018.
- [4] Yi-Lei Chen and Chiou-Ting Hsu. A generalized low-rank appearance model for spatio-temporally correlated rain streaks. In *Proceedings of the IEEE International Conference on Computer Vision*, pages 1968–1975, 2013.
- [5] Marius Cordts, Mohamed Omran, Sebastian Ramos, Timo Rehfeld, Markus Enzweiler, Rodrigo Benenson, Uwe Franke, Stefan Roth, and Bernt Schiele. The cityscapes dataset for semantic urban scene understanding. In *Proc. of the IEEE Conference on Computer Vision and Pattern Recognition (CVPR)*, 2016.
- [6] Liang-Jian Deng, Ting-Zhu Huang, Xi-Le Zhao, and Tai-Xiang Jiang. A directional global sparse model for single image rain removal. *Applied Mathematical Modelling*, 59:662–679, 2018.
- [7] Sen Deng, Mingqiang Wei, Jun Wang, Yidan Feng, Luming Liang, Haoran Xie, Fu Lee Wang, and Meng Wang. Detail-recovery image deraining via context aggregation networks. In *Proceedings of the IEEE/CVF Conference on Computer Vision and Pattern Recognition*, pages 14560–14569, 2020.
- [8] Zhiwen Fan, Huafeng Wu, Xueyang Fu, Yue Huang, and Xinghao Ding. Residual-guide network for single image deraining. In *Proceedings of the 26th ACM international conference on Multimedia*, pages 1751–1759, 2018.
- [9] Xueyang Fu, Jiabin Huang, Delu Zeng, Yue Huang, Xinghao Ding, and John Paisley. Removing rain from single images via a deep detail network. In *Proceedings of the IEEE Conference on Computer Vision and Pattern Recognition*, pages 3855–3863, 2017.
- [10] Tiantong Guo, Hojjat Seyed Mousavi, Tiep Huu Vu, and Vishal Monga. Deep wavelet prediction for image super-resolution. In *Proceedings of the IEEE Conference on Computer Vision and Pattern Recognition Workshops*, pages 104–113, 2017.
- [11] Jie Hu, Li Shen, and Gang Sun. Squeeze-and-excitation networks. In *Proceedings of the IEEE conference on computer vision and pattern recognition*, pages 7132–7141, 2018.
- [12] Xiaowei Hu, Chi-Wing Fu, Lei Zhu, and Pheng-Ann Heng. Depth-attentional features for single-image rain removal. In *Proceedings of the IEEE Conference on Computer Vision and Pattern Recognition*, pages 8022–8031, 2019.
- [13] Kui Jiang, Zhongyuan Wang, Peng Yi, Chen Chen, Baojin Huang, Yimin Luo, Jiayi Ma, and Junjun Jiang. Multi-scale progressive fusion network for single image deraining. In *Proceedings of the IEEE/CVF Conference on Computer Vision and Pattern Recognition*, pages 8346–8355, 2020.
- [14] Li-Wei Kang, Chia-Wen Lin, and Yu-Hsiang Fu. Automatic single-image-based rain streaks removal via image decomposition. *IEEE transactions on image processing*, 21(4):1742–1755, 2011.
- [15] Guanbin Li, Xiang He, Wei Zhang, Huiyou Chang, Le Dong, and Liang Lin. Non-locally enhanced encoder-decoder network for single image de-raining. In *Proceedings of the 26th ACM international conference on Multimedia*, pages 1056–1064, 2018.
- [16] Ruoteng Li, Loong-Fah Cheong, and Robby T Tan. Heavy rain image restoration: Integrating physics model and conditional adversarial learning. In *Proceedings of the IEEE Conference on Computer Vision and Pattern Recognition*, pages 1633–1642, 2019.
- [17] Xia Li, Jianlong Wu, Zhouchen Lin, Hong Liu, and Hongbin Zha. Recurrent squeeze-and-excitation context aggregation net for single image deraining. In *Proceedings of the European Conference on Computer Vision (ECCV)*, pages 254–269, 2018.
- [18] Yu Li, Robby T Tan, Xiaojie Guo, Jiangbo Lu, and Michael S Brown. Rain streak removal using layer priors. In *Proceedings of the IEEE conference on computer vision and pattern recognition*, pages 2736–2744, 2016.
- [19] Bee Lim, Sanghyun Son, Heewon Kim, Seungjun Nah, and Kyoung Mu Lee. Enhanced deep residual networks for single image super-resolution. In *Proceedings of the IEEE conference on computer vision and pattern recognition workshops*, pages 136–144, 2017.
- [20] Pengju Liu, Hongzhi Zhang, Kai Zhang, Liang Lin, and Wangmeng Zuo. Multi-level wavelet-cnn for image restoration. In *Proceedings of the IEEE Conference on Computer Vision and Pattern Recognition Workshops*, pages 773–782, 2018.
- [21] Yu Luo, Yong Xu, and Hui Ji. Removing rain from a single image via discriminative sparse coding. In *Proceedings of the IEEE International Conference on Computer Vision*, pages 3397–3405, 2015.
- [22] Piotr Porwik and Agnieszka Lisowska. The haar-wavelet transform in digital image processing: its status and achievements. *Machine graphics and vision*, 13(1/2):79–98, 2004.
- [23] Rui Qian, Robby T Tan, Wenhan Yang, Jiajun Su, and Jiaying Liu. Attentive generative adversarial network for rain-drop removal from a single image. In *Proceedings of the IEEE conference on computer vision and pattern recognition*, pages 2482–2491, 2018.
- [24] Dongwei Ren, Wangmeng Zuo, Qinghua Hu, Pengfei Zhu, and Deyu Meng. Progressive image deraining networks: a better and simpler baseline. In *Proceedings of the IEEE Conference on Computer Vision and Pattern Recognition*, pages 3937–3946, 2019.
- [25] Olaf Ronneberger, Philipp Fischer, and Thomas Brox. U-net: Convolutional networks for biomedical image segmentation. In *International Conference on Medical image computing and computer-assisted intervention*, pages 234–241. Springer, 2015.
- [26] Liang Shen, Zihan Yue, Quan Chen, Fan Feng, and Jie Ma. Deep joint rain and haze removal from a single image. In *2018 24th International Conference on Pattern Recognition (ICPR)*, pages 2821–2826. IEEE, 2018.
- [27] Ke Sun, Bin Xiao, Dong Liu, and Jingdong Wang. Deep high-resolution representation learning for human pose estimation. In *Proceedings of the IEEE Conference on Computer Vision and Pattern Recognition*, pages 5693–5703, 2019.

- [28] Mingxing Tan, Ruoming Pang, and Quoc V Le. Efficientdet: Scalable and efficient object detection. *arXiv preprint arXiv:1911.09070*, 2019.
- [29] Ludovic Trottier, Philippe Gigu, Brahim Chaib-draa, et al. Parametric exponential linear unit for deep convolutional neural networks. In *2017 16th IEEE International Conference on Machine Learning and Applications (ICMLA)*, pages 207–214. IEEE, 2017.
- [30] Guoqing Wang, Changming Sun, and Arcot Sowmya. Erl-net: Entangled representation learning for single image de-raining. In *Proceedings of the IEEE International Conference on Computer Vision*, pages 5644–5652, 2019.
- [31] Hong Wang, Qi Xie, Qian Zhao, and Deyu Meng. A model-driven deep neural network for single image rain removal. In *Proceedings of the IEEE/CVF Conference on Computer Vision and Pattern Recognition*, pages 3103–3112, 2020.
- [32] Jingdong Wang, Ke Sun, Tianheng Cheng, Borui Jiang, Chaorui Deng, Yang Zhao, Dong Liu, Yadong Mu, Mingkui Tan, Xinggang Wang, et al. Deep high-resolution representation learning for visual recognition. *arXiv preprint arXiv:1908.07919*, 2019.
- [33] Tianyu Wang, Xin Yang, Ke Xu, Shaozhe Chen, Qiang Zhang, and Rynson WH Lau. Spatial attentive single-image deraining with a high quality real rain dataset. In *Proceedings of the IEEE Conference on Computer Vision and Pattern Recognition*, pages 12270–12279, 2019.
- [34] Xiaolong Wang, Ross Girshick, Abhinav Gupta, and Kaiming He. Non-local neural networks. In *The IEEE Conference on Computer Vision and Pattern Recognition (CVPR)*, June 2018.
- [35] Yinglong Wang, Shuaicheng Liu, Chen Chen, and Bing Zeng. A hierarchical approach for rain or snow removing in a single color image. *IEEE Transactions on Image Processing*, 26(8):3936–3950, 2017.
- [36] Yinglong Wang, Yibing Song, Chao Ma, and Bing Zeng. Rethinking image deraining via rain streaks and vapors. *arXiv preprint arXiv:2008.00823*, 2020.
- [37] Wenhan Yang, Jiaying Liu, Shuai Yang, and Zongming Guo. Scale-free single image deraining via visibility-enhanced recurrent wavelet learning. *IEEE Transactions on Image Processing*, 28(6):2948–2961, 2019.
- [38] Wenhan Yang, Robby T Tan, Jiashi Feng, Jiaying Liu, Zongming Guo, and Shuicheng Yan. Deep joint rain detection and removal from a single image. In *Proceedings of the IEEE Conference on Computer Vision and Pattern Recognition*, pages 1357–1366, 2017.
- [39] Wenhan Yang, Robby T Tan, Shiqi Wang, Yuming Fang, and Jiaying Liu. Single image deraining: From model-based to data-driven and beyond. *arXiv preprint arXiv:1912.07150*, 2019.
- [40] Wenhan Yang, Shiqi Wang, Dejie Xu, Xiaodong Wang, and Jiaying Liu. Towards scale-free rain streak removal via self-supervised fractal band learning. In *AAAI*, pages 12629–12636, 2020.
- [41] Jaejun Yoo, Namhyuk Ahn, and Kyung-Ah Sohn. Rethinking data augmentation for image super-resolution: A comprehensive analysis and a new strategy. *arXiv preprint arXiv:2004.00448*, 2020.
- [42] Weijiang Yu, Zhe Huang, Wayne Zhang, Litong Feng, and Nong Xiao. Gradual network for single image de-raining. In *Proceedings of the 27th ACM International Conference on Multimedia*, pages 1795–1804, 2019.
- [43] Sangdoon Yun, Dongyoon Han, Seong Joon Oh, Sanghyuk Chun, Junsuk Choe, and Youngjoon Yoo. Cutmix: Regularization strategy to train strong classifiers with localizable features. In *Proceedings of the IEEE International Conference on Computer Vision*, pages 6023–6032, 2019.
- [44] He Zhang and Vishal M Patel. Density-aware single image de-raining using a multi-stream dense network. In *Proceedings of the IEEE conference on computer vision and pattern recognition*, pages 695–704, 2018.
- [45] He Zhang, Vishwanath Sindagi, and Vishal M Patel. Image de-raining using a conditional generative adversarial network. *IEEE transactions on circuits and systems for video technology*, 2019.
- [46] Kaihao Zhang, Wenhan Luo, Wenqi Ren, Jingwen Wang, Fang Zhao, Lin Ma, and Hongdong Li. Beyond monocular deraining: Stereo image deraining via semantic understanding. In *European Conference on Computer Vision (ECCV)*, 2020.
- [47] Yulun Zhang, Kunpeng Li, Kai Li, Lichen Wang, Bineng Zhong, and Yun Fu. Image super-resolution using very deep residual channel attention networks. In *Proceedings of the European Conference on Computer Vision (ECCV)*, pages 286–301, 2018.
- [48] Lei Zhu, Chi-Wing Fu, Dani Lischinski, and Pheng-Ann Heng. Joint bi-layer optimization for single-image rain streak removal. In *Proceedings of the IEEE international conference on computer vision*, pages 2526–2534, 2017.